JCI The Journal of Clinical Investigation

High salt intake reprioritizes osmolyte and energy metabolism for body fluid conservation

Kento Kitada, Steffen Daub, Yahua Zhang, Janet D. Klein, Daisuke Nakano, Tetyana Pedchenko, Louise Lantier, Lauren M. LaRocque, Adriana Marton, Patrick Neubert, Agnes Schröder, Natalia Rakova, Jonathan Jantsch, Anna E. Dikalova, Sergey I. Dikalov, David G. Harrison, Dominik N. Müller, Akira Nishiyama, Manfred Rauh, Raymond C. Harris, Friedrich C. Luft, David H. Wassermann, Jeff M. Sands, Jens Titze

J Clin Invest. 2017;127(5):1944-1959. https://doi.org/10.1172/JCI88532.

Research Article **Metabolism** **Nephrology**

Natriuretic regulation of extracellular fluid volume homeostasis includes suppression of the renin-angiotensin-aldosterone system, pressure natriuresis, and reduced renal nerve activity, actions that concomitantly increase urinary Na^+ excretion and lead to increased urine volume. The resulting natriuresis-driven diuretic water loss is assumed to control the extracellular volume. Here, we have demonstrated that urine concentration, and therefore regulation of water conservation, is an important control system for urine formation and extracellular volume homeostasis in mice and humans across various levels of salt intake. We observed that the renal concentration mechanism couples natriuresis with correspondent renal water reabsorption, limits natriuretic osmotic diuresis, and results in concurrent extracellular volume conservation and concentration of salt excreted into urine. This water-conserving mechanism of dietary salt excretion relies on urea transporter–driven urea recycling by the kidneys and on urea production by liver and skeletal muscle. The energy-intense nature of hepatic and extrahepatic urea osmolyte production for renal water conservation requires reprioritization of energy and substrate metabolism in liver and skeletal muscle, resulting in hepatic ketogenesis and glucocorticoid-driven muscle catabolism, which are prevented by increasing food intake. This natriuretic-ureotelic, water-conserving principle relies on metabolism-driven extracellular volume control and is regulated by concerted liver, muscle, and renal actions.

High salt intake reprioritizes osmolyte and energy metabolism for body fluid conservation

Kento Kitada,[1] Steffen Daub,[1,2] Yahua Zhang,[1] Janet D. Klein,[3,4] Daisuke Nakano,[5] Tetyana Pedchenko,[1] Louise Lantier,[6] Lauren M. LaRocque,[3,4] Adriana Marton,[1] Patrick Neubert,[7] Agnes Schröder,[7] Natalia Rakova,[8] Jonathan Jantsch,[9] Anna E. Dikalova,[1] Sergey I. Dikalov,[1] David G. Harrison,[1] Dominik N. Müller,[8] Akira Nishiyama,[5] Manfred Rauh,[10] Raymond C. Harris,[11] Friedrich C. Luft,[1,8] David H. Wassermann,[6] Jeff M. Sands,[3,4] and Jens Titze[1,7]

[1]Division of Clinical Pharmacology, Vanderbilt University Medical Center, Nashville, Tennessee, USA. [2]Department of Medicine II, University Medical Center Mainz, Mainz, Germany. [3]Renal Division, Department of Medicine, and [4]Department of Physiology, Emory University, Atlanta, Georgia, USA. [5]Department of Pharmacology, Faculty of Medicine, Kagawa University, Kagawa, Japan. [6]Department of Molecular Physiology and Biophysics, Vanderbilt University, Nashville, Tennessee, USA. [7]Junior Research Group 2, Interdisciplinary Center for Clinical Research, University Clinic Erlangen, Erlangen, Germany. [8]Experimental and Clinical Research Center, Charité Medical Faculty and the Max-Delbrueck Center for Molecular Medicine, Berlin, Germany. [9]Institute of Clinical Microbiology and Hygiene, University Clinic Regensburg and University Regensburg, Regensburg, Germany. [10]Department of Pediatrics, University Clinic Erlangen, Erlangen, Germany. [11]Division of Nephrology and Hypertension, Vanderbilt University Medical Center, Nashville, Tennessee, USA.

Natriuretic regulation of extracellular fluid volume homeostasis includes suppression of the renin-angiotensin-aldosterone system, pressure natriuresis, and reduced renal nerve activity, actions that concomitantly increase urinary Na^+ excretion and lead to increased urine volume. The resulting natriuresis-driven diuretic water loss is assumed to control the extracellular volume. Here, we have demonstrated that urine concentration, and therefore regulation of water conservation, is an important control system for urine formation and extracellular volume homeostasis in mice and humans across various levels of salt intake. We observed that the renal concentration mechanism couples natriuresis with correspondent renal water reabsorption, limits natriuretic osmotic diuresis, and results in concurrent extracellular volume conservation and concentration of salt excreted into urine. This water-conserving mechanism of dietary salt excretion relies on urea transporter–driven urea recycling by the kidneys and on urea production by liver and skeletal muscle. The energy-intense nature of hepatic and extrahepatic urea osmolyte production for renal water conservation requires reprioritization of energy and substrate metabolism in liver and skeletal muscle, resulting in hepatic ketogenesis and glucocorticoid-driven muscle catabolism, which are prevented by increasing food intake. This natriuretic-ureotelic, water-conserving principle relies on metabolism-driven extracellular volume control and is regulated by concerted liver, muscle, and renal actions.

Introduction

Renal excretion of dietary Na^+ under high-salt conditions occurs by a natriuretic principle. The assumption is that high salt intake triggers thirst and thereby increases fluid intake, which expands the extracellular fluid volume. Successful renal excretion of excess salt conversely increases the urine volume by osmotic diuresis and thereby corrects the extracellular volume (1–3). According to the established concept, high salt intake increases fluid intake. Subsequent renal elimination of surplus dietary salt is used to excrete the parallel surplus water load and reduce the expanded extracellular volume back to normal.

In an ultra-long-term Na^+ and water balance study of 10 healthy humans (4), we found that increasing dietary salt intake paradoxically decreased fluid intake in all test subjects. The result has caused us to reinvestigate the accepted concept that increased salt intake leads to parallel increases in Na^+ and water intake and excretion. We studied the physiological role of the renal concentration mechanism during high salt intake, which is characterized by excretion of surplus dietary salt and antiparallel water movement for renal water conservation while the salt osmolytes are excreted. We show that urea metabolism plays an important role in extracellular volume control by maintaining the renal concentration mechanism during high salt intake. In this study, mice given a high-salt diet increased urea osmolyte production and recycling to provide the osmotic driving force that allows excretion of dietary salt without major changes in urine volume. The physiological response of this water conservation process during salt excretion can be summarized as natriuretic-ureotelic regulation for endogenous free water accrual within the renal urine concentration process to prevent body water loss. In addition, salt can induce a glucocorticoid-driven catabolic state with increased urea osmolyte and metabolic water generation.

▶ Related Article: p. 1932
▶ Related Commentary: p. 1625

Authorship note: K. Kitada and S. Daub contributed equally to this work.
Conflict of interest: The authors have declared that no conflict of interest exists.
Submitted: May 17, 2016; **Accepted:** February 17, 2017.
Reference information: *J Clin Invest*. 2017;127(5):1944–1959.
https://doi.org/10.1172/JCI88532.

Results

Surplus osmolyte and water excretion by urine concentration in mice and humans. We fed C57/BL6 mice either a low-salt diet (0.1%

Table 1. Effect of increasing salt intake on urine osmolyte, volume, and glucocorticoid-hormone excretion in balance studies in mice and humans

	Mouse balance studies				Human balance study	
	LS	HS + saline	LS	HS + tap	6 g/d	12 g/d
Number of subjects	(*n* = 6)	(*n* = 8)	(*n* = 7)	(*n* = 7)	(*n* = 10)	(*n* = 10)
Osmolyte excretion	(*n* = 6)	(*n* = 8)	(*n* = 7)	(*n* = 7)	(*n* = 396)	(*n* = 739)
UNaV (mmol/kg/d)	1.3 ± 0.4	13 ± 5.5[A]	2.1 ± 0.9	11 ± 3.0[A]	1.2 ± 0.4	2.3 ± 0.5[A]
UKV (mmol/kg/d)	10 ± 1.9	6.6 ± 1.6[A]	9.3 ± 1.4	6.0 ± 1.6[A]	1.0 ± 0.3	1.1 ± 0.3[A]
UUreaV (mmol/kg/d)	53 ± 12	49 ± 11	42 ± 7.9	42 ± 11.3	4.3 ± 1.0	4.1 ± 1.1[A]
U2Na2KUreaV (mmol/kg/d)	76 ± 15	89 ± 22	65 ± 10	75 ± 19	8.6 ± 2.1	10.8±2.3[A]
Osmolyte concentration	(*n* = 6)	(*n* = 8)	(*n* = 7)	(*n* = 7)	(*n* = 404)	(*n* = 740)
U[Na^+] (mmol/l)	19 ± 7	148 ± 32[A]	32 ± 10	130 ± 26[A,E]	56 ± 24	108 ± 34[A]
U[K^+] (mmol/l)	151 ± 20	78 ± 18[A]	147 ± 13	73 ± 12[A]	50 ± 22	54 ± 21[A]
U[Urea] (mmol/l)	780 ± 112	575 ± 127[A]	665 ± 149	522 ± 81[A]	217 ± 99	197 ± 76[A]
U[2Na^+2K^+Urea] (mmol/l)	1,120 ± 157	1,026 ± 148	1,024 ± 168	930 ± 124	430 ± 177	520 ± 170[A]
Urine osmolality (mOsm/kg)	984 ± 126	895 ± 120	958 ± 146	834 ± 124	431 ± 175	508 ± 170[A]
Fluid intake and urine volume	(*n* = 6)	(*n* = 8)	(*n* = 7)	(*n* = 7)	(*n* = 396)	(*n* = 739)
Urine volume (ml/kg/d)	69 ± 15	89 ± 28	64 ± 13	81 ± 17[B]	22 ± 8	22 ± 7
Fluid intake (ml/kg/d)	48 ± 12	37 ± 14	35 ± 18	55 ± 19[B,D]	35 ± 7	31 ± 7[A]
FWC (ml/kg/d)	–154 ± 29	–169 ± 36	–138 ± 26	–143 ± 41	–6.6 ± 8.7	–12.6 ± 7.6[A]
Urine glucocorticoid excretion[F]	(*n* = 6)	(*n* = 6)	(*n* = 6)	(*n* = 6)	(*n* = 404)	(*n* = 742)
	30 ± 7	40 ± 8[A]	33 ± 4	31 ± 5[C,D]	18 ± 6	24 ± 8[A]

Studies in mice: Mice were fed a LS diet (0.1% NaCl chow with tap water) or a HS diet (4% NaCl chow with either 0.9% saline water or, alternatively, tap water to drink) and were placed into metabolic cages for 24 hours with either tap water or saline water to drink, without food. Data were analyzed by multivariate analysis (general linear model). Human studies: 10 healthy men monitored their fluid intake and collected 24-hour urine samples for 6-g/d or 12-g/d salt intake in ultra-long-term Na^+ balance studies of 105 and 205 days' duration. Data were determined by mixed-linear model analysis and are expressed as the average ± the SD. [A]$P_{(salt)} < 0.05$; [B]$P_{(salt)} < 0.1$, [C]$P_{(free\ access\ to\ water)} < 0.05$; [D]$P_{(interaction\ between\ salt\ and\ free\ access\ to\ water)} < 0.05$; and [E]$P_{(interaction\ between\ salt\ and\ free\ access\ to\ water)} < 0.1$. Osmolyte excretion is given per 24-hour urine volume (UV). [F]Glucocorticoid excretion in humans was quantified by 24-hour cortisol excretion (μg/d); glucocorticoid excretion in mice was quantified by 24-hour corticosterone excretion (ng/d).

NaCl chow and tap water to drink, referred to herein as LS) or a high-salt diet (4% NaCl chow and 0.9% saline water to drink; referred to herein as HS+saline) for 2 consecutive weeks and studied their 24-hour water balance in metabolic cages. To prevent artificial osmolyte contamination of the urine, the mice received their assigned fluids without food during the 24-hour urine collection period. We also measured the animals' food and fluid intake in normal cages in the 24-hour period before their transfer to the metabolic cages. In the normal cages, daily average food intake was 154 ± 22 g/kg body weight, corresponding to 12 kg in an 80-kg human. The average fluid intake was 506 ± 281 ml/kg, corresponding to 40 liters in an 80-kg human. The HS+saline diet not only increased fluid intake by 3.1-fold (714 ± 170 ml/kg versus 228 ± 48 ml/kg; $P < 0.001$), but also led to a 1.2-fold increase in food intake (165 ± 21 g/kg versus 140 ± 15 g/kg; $P < 0.05$). The large nutrient intake suggests that not only surplus Na^+ but also large amounts of K^+ and urea osmolytes were excreted together with surplus water.

Food and water intake of the previous day dominated fluid intake behavior and osmolyte and water excretion in the subsequent 24-hour metabolic cage studies. It was not fluid intake on the same day, but fluid intake on the previous day that determined urine volume formation in the metabolic cage experiments (Supplemental Figure 1, A and B; supplemental material available online with this article; https://doi.org/10.1172/JCI88532DS1). Furthermore, the higher fluid intake in the HS+saline mice in the normal cage determined lower fluid intake in the same mice during the subsequent metabolic cage experiment (Supplemental Figure 1C). This state of affairs confirmed the hypothesis that the surplus body fluid generated earlier was excreted in the metabolic cage experiments.

Despite a 10-fold increase in urine Na^+ excretion (UNaV), HS+saline mice showed no significant increase in total osmolyte excretion (Table 1). Urea was the dominating urine osmolyte, being 40-fold higher than urine Na^+ in LS diet–fed mice and 4-fold higher than urine Na^+ in HS+saline diet–fed mice. The sum of $2Na^+$ (2-fold to account for accompanying anions), $2K^+$ (2-fold to account for accompanying anions), and urea excretion (U2Na2KUreaV; mmol/kg/d) was dependent on the previous day's food intake (Supplemental Figure 2), indicating that Na^+ salts, K^+ salts, and predominantly protein intake determined surplus urine osmolyte excretion in mice in the metabolic cage 24 hours later.

Despite a massive difference in UNaV, neither LS- nor HS+saline-treated mice showed a significant increase in urine volume (Table 1), indicating that surplus water excretion was not proportional to surplus Na^+ excretion. This disproportional Na^+ and water excretion was explained by the finding that HS+saline mice showed an 8-fold increase in their urine Na^+ concentration. Excretion of surplus dietary salt and water thus occurred within the physiological regulatory pattern of the renal concentration mechanism. In the renal excretion process, proportional amounts of osmolytes and water are first filtered from the blood plasma into the primary urine. The hyperosmolal microenvironment in the renal interstitium then drives water reabsorption and, thereby, urine concentration. This antidromic movement of osmolytes and water can be assessed by calculating the negative free water clearance (FWC), which is an estimate of renal tubular water reabsorption in relation to osmolyte excretion. The average FWC in LS and HS+saline mice was –162 ml/kg/d (Table 1), which would correspond to water conservation of approximately 13 l/d by renal osmolyte free water reabsorption in an 80-kg human.

Dietary salt excretion did not change urine osmolality or FWC, because the 25.7% increase in urine $2Na^+$ concentration was balanced by a 11.7% reduction in urine $2K^+$ concentration and a

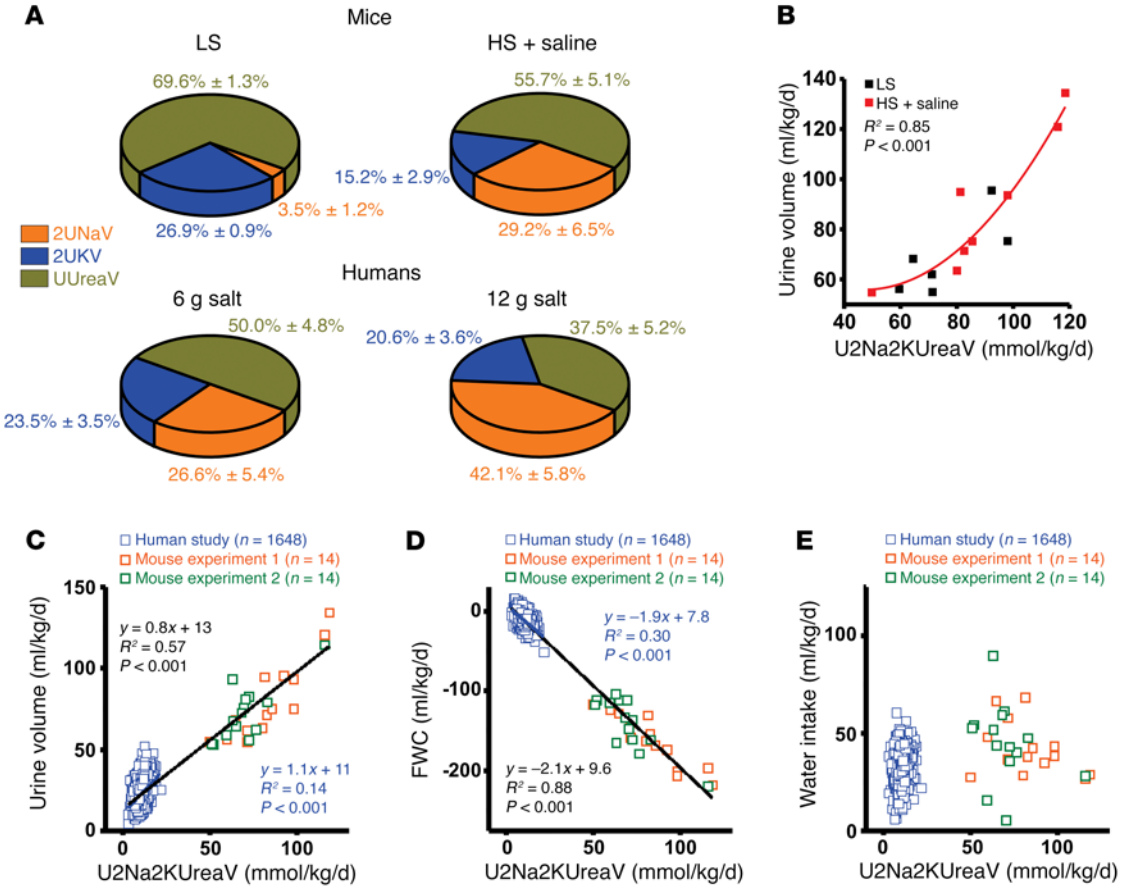

Figure 1. Natriuretic-ureotelic generation of urine volume by surplus osmolyte and water excretion in mice and in humans. (**A**) Relative contribution of 24-hour Na^+ (2UNaV), K^+ (2UKV), and urea (UUreaV) excretion to total 24-hour Na^+, K^+, and urea osmolyte excretion in mice on a LS diet (n = 6) or a HS diet with isotonic saline to drink (HS+saline; n = 8), and in 10 men consuming a 6-g/d or 12-g/d salt diet. Two-fold values of UNaV and UKV are given to account for their unmeasured accompanying anions. (**B**) Relationship among surplus $2Na^+$, $2K^+$, and urea osmolyte excretion (U2Na2KUreaV) and surplus water excretion in mice on a 0.1% NaCl diet with tap water (LS) (n = 6) or a 4% NaCl diet with 0.9% saline (HS+saline) (n = 8) for 2 consecutive weeks. (**C**) Relationship between surplus U2Na2KUreaV and surplus water excretion in all mice and human subjects presented in Table 1. (**D**) Relationship between surplus U2Na2KUreaV and FWC in the same mice and human subjects. (**E**) Relationship between surplus U2Na2KUreaV and water intake in the same mice and human subjects. We performed regression analysis in humans, and across the species. Mouse experiment 1: HS+saline study; mouse experiment 2: HS+tap study.

13.9% reduction in urine urea concentration (Table 1 and Figure 1A). This finding suggests that K^+ and urea osmolytes provided the primary osmotic driving force necessary to reabsorb water and concentrate excess dietary Na^+ osmolytes into the urine. Urine formation by total surplus osmolyte and water excretion showed the expected close relationship between U2Na2KUreaV and water excretion (Figure 1B). These findings indicate that in HS+saline mice, further increase in urine volume were prevented by K^+- and urea-driven maintenance of the renal concentration mechanism, thereby preventing Na^+-driven extracellular volume loss.

We next tested the reproducibility of our findings in additional experiments in mice with dietary salt loading and free access to water (4% NaCl chow and tap water; HS+tap) and compared the responses with results from 10 human subjects whose salt intake was increased by 6 g/d during two 105-day and 205-day ultra-long-term salt and water balance studies (4). Surplus Na^+ and K^+ excretion was 5-fold higher and surplus urea excretion was 10-fold higher in the mice than in the human subjects (Table 1). Accounting for unmeasured anions, surplus osmolyte excretion was 7-fold higher in mice than in humans, while surplus water excretion was 3-fold higher. The mice thus had a 2-fold higher urine osmolality than did the human subjects. Endogenous free water accrual by negative FWC in the kidney was therefore 15-fold higher in the mice than in the human subjects (Table 1). Despite these substantial differences in body osmolyte and water homeostasis and across the different dietary salt interventions, the mice and human subjects shared the natriuretic-ureotelic regulatory principle of excreting surplus dietary salt by concentrating Na^+ into the urine and in parallel reducing the urine urea concentration (Table 1).

Independent of the salt intake level, mice and humans eliminated surplus Na^+, K^+, and urea osmolytes with increasing amounts of surplus water (Figure 1C). Across the species and the different salt-intake protocols increased surplus osmolyte excretion was characterized by increased urine concentration and, thus, by reduced clearance of free water (Figure 1D). This finding indicates that the biological and physiological pattern of extracellular volume control during surplus osmolyte excretion substantially relies on water conservation by urine concentration.

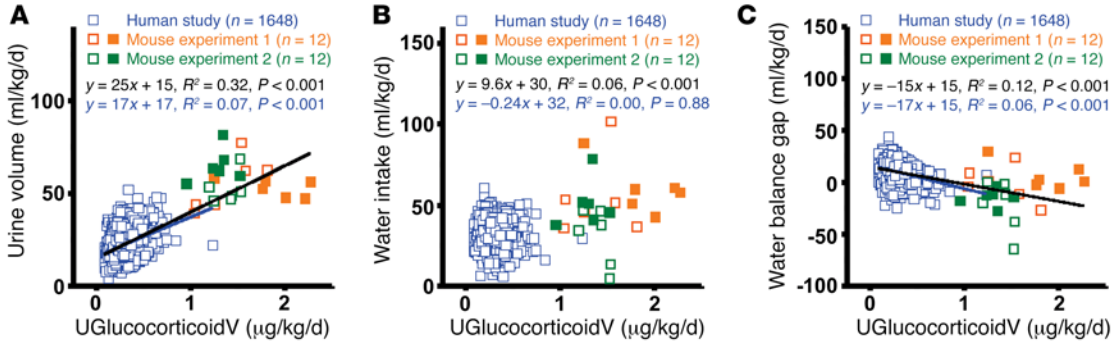

Figure 2. Glucocorticoid levels and water balance in mice and humans. (**A**) Relationship between glucocorticoid (UGlucocorticoidV) levels and water excretion in the urine for all mice and human subjects presented in Table 1. (**B**) Relationship between glucocorticoid levels and water intake in the same mice. (**C**) Relationship between glucocorticoid levels and water balance in the same mice. Regression analysis was performed for humans and across the species. Mouse experiment 1: HS+saline study; mouse experiment 2: HS+tap study.

Extracellular volume control in the mice and human subjects with increasing osmolyte excretion was therefore not dependent on a parallel adjustment of fluid intake (Figure 1E). A 6-g/d increase in salt intake reduced FWC in humans, and the resulting increase in endogenous free water accrual resulted in surplus water excretion and reduced fluid intake (see Table 1 and the accompanying article [ref. 4] for details). This water intake and excretion pattern was best simulated in our metabolic cage experiments involving HS+saline mice (Table 1).

Glucocorticoid-coupled surplus water excretion and its association with dietary salt loading in mice and humans. In our ultra-long-term water balance study in humans, spontaneous rhythmical cortisone release was coupled with increased urine volume formation and increased free water excretion without increasing fluid intake, indicating a rhythmical release of endogenously generated surplus water (see the accompanying article [ref. 4] for details). This finding was reproducible in mice. In humans, increasing cortisol excretion augmented urine volume (Figure 2A) without increasing water intake (Figure 2B), resulting in a negative water balance (water balance gap: difference between water intake and urinary output; Figure 2C) and indicating excretion of surplus water. Relative to body mass, corticosterone levels in the mice in metabolic cages were higher than the cortisol levels detected in the human subjects. These higher glucocorticoid levels were coupled with further increases in urine volume (Figure 2A), while water intake was not similarly increased (Figure 2B), resulting in a negative water balance across the species (Figure 2C).

We hypothesized that dietary salt loading not only promotes urea-driven free water accrual within the renal urine concentration process to prevent a negative water balance, but additionally induces glucocorticoid-driven catabolism for metabolic urea osmolyte generation and increased metabolic water production. We tested these hypotheses in HS+saline mice, which, like the human subjects, showed increased glucocorticoid levels in response to the dietary salt–loading protocol (Table 1).

Dietary salt induces urea transporter–driven urea osmolyte accumulation in the kidney. After 6 weeks on their specified diets, the LS and HS+saline mice were studied to determine the inner medullary urea content and expression of the outer medullary urea transporter UT-A2 and the inner medullary urea transporter UT-A1 (Figure 3, A–C, and see Supplemental Figure 3, A and B, for the complete, unedited Western blots). We found a marked increase in medullary urea content in the HS+saline mice, which was paralleled by increased UT-A1 expression. We interpret these findings as showing that UT-A1–driven urea accumulation in the renal medulla provides the osmotic gradient necessary to reabsorb water when dietary salt is excreted. This water-saving effect of urea osmolyte accumulation is the basis of the concentration mechanism, whereby the kidney excretes salt without major changes in fluid intake or urinary water loss. HS+tap-treated mice showed a similar urine osmolyte excretion and concentration profile (Table 1) and similar increases in UT-A1 expression in the renal medulla (Supplemental Figure 3, C and D), but no increased glucocorticoid excretion. This finding indicates that the renal natriuretic-ureotelic response was also triggered when free access to water was offered in the diet and that increasing glucocorticoid levels was not necessary to induce the urea-driven renal water conservation process.

Urea and Na^+ hold water in the plasma space. We next tested the hypothesis that renal medullary urea accumulation not only facilitates renal water reabsorption but also changes plasma urea concentration. We found that HS+saline treatment significantly increased the plasma urea concentration (Figure 3D). Treatment with the unspecific arginase inhibitor N-ω-hydroxy-L-norarginine (NOHA) left plasma urea levels unchanged. Conversely, HS+saline decreased plasma Na^+ concentrations, while NOHA treatment left plasma Na^+ levels unchanged (Figure 3E). Plasma osmolality was not different between HS+saline- and HS+saline+NOHA-treated mice (Figure 3F). We conclude that both urea and Na^+ act as osmolytes to conserve plasma water and thereby contribute to extracellular volume regulation. NOHA did not significantly reduce renal UT-A1 or UT-A2 expression (Figure 3, B and C, and see Supplemental Figure 3, A and B, for the complete, unedited Western blots). This finding suggests that, besides transporter-driven renal urea recycling, extrarenal urea osmolyte production may play an important role in extracellular volume control.

Extrarenal urea generation is a determinant of plasma urea concentration. We thus tested the relationship among arginase activity, tissue urea content, and plasma urea levels. HS+saline increased renal medullary urea content and plasma urea concentration (Figure 4A); however, this increase was not dependent on renal argin-

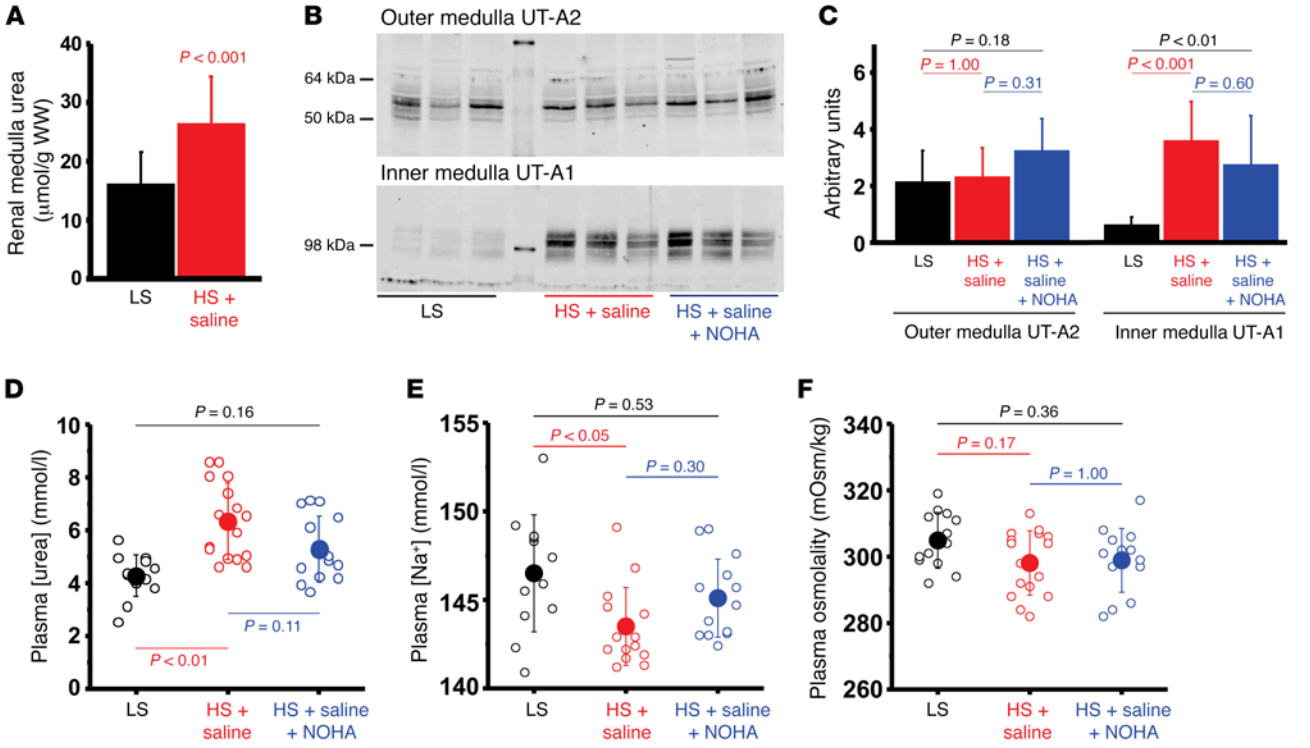

Figure 3. Renal urea accumulation, plasma Na^+ and urea concentration, and plasma osmolality in response to experimental salt loading. (**A**) Urea content in the renal medulla in mice that received less than 0.1% salt and tap water (LS; $n = 6$) or 4% salt and 0.9% saline (HS+saline; $n = 7$). (**B**) Representative UT-A1 and UT-A2 expression in the outer medulla and inner medulla of mice on a LS ($n = 3$), HS+saline ($n = 3$), or HS+saline+NOHA ($n = 3$) diet. (**C**) Quantification of UT-A1 and UT-A2 expression in the outer and inner medullae of mice on a LS ($n = 8$), HS+saline ($n = 8$), or HS+saline+NOHA ($n = 8$) diet. (**D**) Plasma urea concentration in mice on a LS ($n = 14$), HS+saline ($n = 16$), or HS+saline+NOHA ($n = 14$) diet. (**E**) Plasma Na^+ concentration in mice on a LS ($n = 12$), HS+saline ($n = 15$), or HS+saline+NOHA ($n = 14$) diet. (**F**) Plasma osmolality in mice on a LS diet ($n = 13$), HS+saline diet ($n = 16$), or a HS+saline diet plus NOHA treatment (HS+saline+NOHA; $n = 14$). Data were determined by multivariate analysis (general linear model) and Bonferroni's post-hoc subgroup comparisons.

ase activity, suggesting that the observed decrease in medullary urea content and plasma urea concentration in NOHA-treated mice was most likely due to reduced extrarenal urea production. Therefore, we next studied the role of urea production in the liver (Figure 4B). HS+saline increased hepatic arginase activity and thereby increased urea content in the liver. We found that liver urea content was a better predictor of plasma urea levels than was renal medullary urea content. In contrast to what we observed in kidney, liver arginase activity strongly predicted liver urea content and plasma urea concentration. NOHA treatment reduced liver arginase activity and, in parallel, reduced liver urea content as well as the plasma urea concentration. We interpret this finding as showing that liver and kidney jointly control body osmolyte content and thereby determine extracellular volume homeostasis. We also found that HS+saline increased arginase activity and urea content in skeletal muscle (Figure 4C). NOHA treatment reduced muscle urea content back to the control values. This finding suggests that the increase in muscle urea content was due to local urea production in the muscle, indicating additional extrahepatic urea generation.

Salt leads to catabolic muscle mass loss. We next tested the hypothesis that salt-driven urea osmolyte generation induces a catabolic state and studied the effect of dietary salt loading on the respiratory quotient (RQ) in the mice. A 4% NaCl diet did not significantly decrease RQ as long as mice had free access to tap water (Figure 5A). Immediately upon replacement of tap water with isotonic saline, HS+saline-treated mice had decreased RQ during the inactive period to a value of 0.7. We interpret these findings as showing that HS+saline induces catabolism with predominant fat oxidation for energy generation in mice. The time course of the changes in food intake and body weight in LS- and HS+saline-treated mice over 4 weeks of ad libitum feeding, followed by 2 weeks of pair-feeding (Figure 5, B and C), revealed that with ad libitum feeding, HS+saline mice showed a 20%–30% increase in food intake. However, body weights remained similar between the groups. We then pair-fed the mice and reduced the food intake of HS+saline diet–fed mice to that of LS diet–fed mice. With pair-feeding, HS+saline mice lost approximately 10% of their total body weight within 1 week. In contrast to salt loading with the HS+saline diet, the HS diet with free access to water neither increased glucocorticoid levels (Table 1), nor increased food intake in the ad libitum food intake phase, nor decreased body weight in the pair-feeding phase (Supplemental Figure 4).

We therefore next hypothesized that the observed weight loss in HS+saline mice after pair-feeding was due to corticosterone-driven loss of muscle mass. We first tested whether elevated corticosterone levels in HS+saline mice led to glucocorticoid receptor (GR) activation in the muscle (Figure 5D, upper panel, Figure 5E, and see Supplemental Figure 5 for the complete, unedited Western blots). HS+saline did not increase GR protein levels in the cytoplasm, the membrane, or in the soluble nuclear frac-

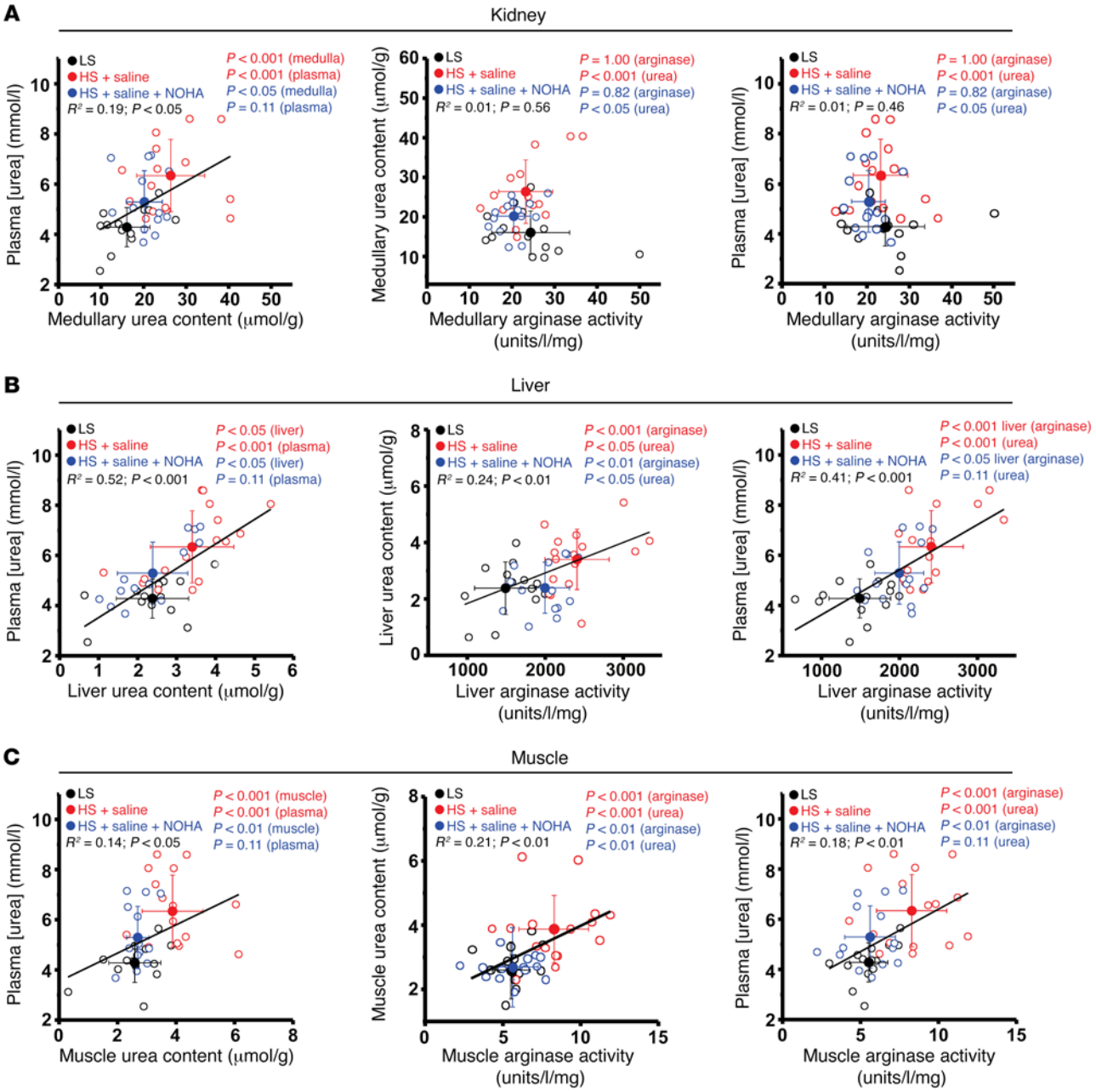

Figure 4. Relationship among tissue urea content, tissue arginase activity, and plasma urea concentration. (**A**) Relationship among renal medullary urea content, renal medullary arginase activity, and plasma urea concentration in mice fed a LS (n = 14), HS+saline (n = 15), or HS+saline+NOHA (n = 14) diet. (**B**) Relationship among liver urea content, liver arginase activity, and plasma urea concentration in the same mice. (**C**) Relationship among muscle urea content, muscle arginase activity, and plasma urea concentration in the same mice. Data were determined by linear regression, multivariate analysis (general linear model), and Bonferroni's post-hoc subgroup comparisons.

tion. In contrast, nuclear chromatin–bound GR protein expression increased with HS+saline, showing GR activation. In parallel with GR activation, microtubule-associated protein 1A/1B chain 3 (LC3, structural precursor protein within the autophagic pathway) was preferentially lipidated from the cytosolic form (LC3-I, cleaved from LC3) to the derivate associated with autophagosome membrane expansion, LC3-II. The resulting increase in the LC3-II/LC3-I ratio (Figure 5D, lower panel, and see Supplemental Figure 6 for the complete, unedited Western blots), which was paralleled by a tendency toward higher levels of autophagy-related protein 5 (*ATG5*, involved in the lipidation of LC3-I to LC3-II) and by reduced levels of the autophagosome carrier protein p62 (*SQSTM1*, sequestosome 1, which targets polyubiquitinated proteins for degradation), indicates increased autophagosome formation (see Supplemental Figure 7, A–C, for the complete, unedited Western blots). Additionally, skeletal muscle in HS+saline mice showed increased 1-methyl histidine and 3-methyl histidine levels, indicating muscle protein breakdown (Supplemental Figure 7D).

Mice given HS+saline had increased chromatin-bound GR protein levels, increased autophagosome formation markers, and

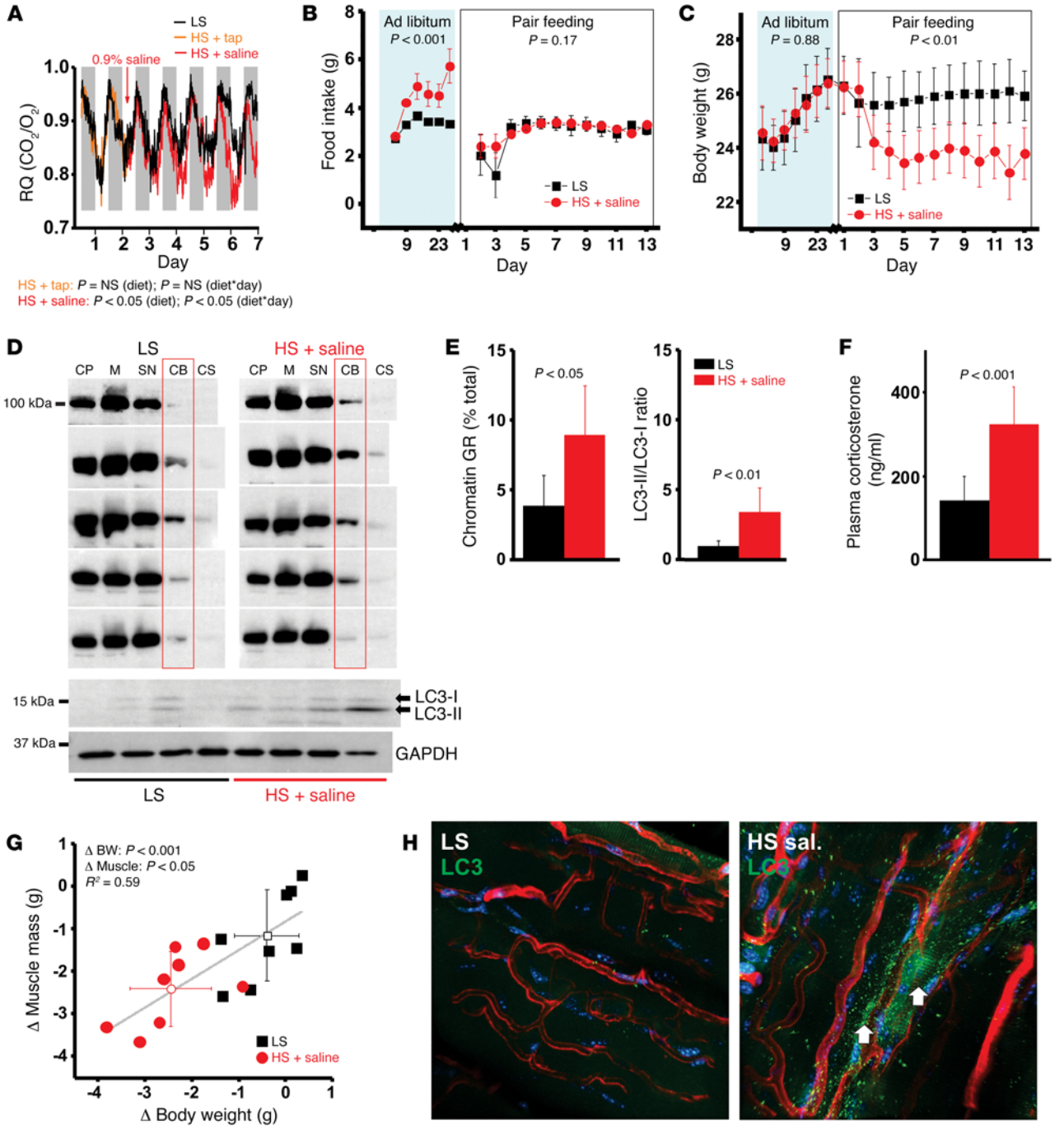

Figure 5. Catabolic muscle wasting by experimental salt loading. (**A**) RQ in mice fed a 0.1% NaCl chow (LS) (n = 8) or a 4% NaCl chow (n = 8) diet for 7 consecutive days. To test the effect of additional isotonic saline, mice received tap water for 2 days (HS+tap, orange), followed by isotonic saline (HS+saline, red). The activity period at night is shown in gray, and the inactivity period during the daytime is shown in white. Food intake (**B**) and body weight (**C**) over a 28-day period of ad libitum feeding, followed by 14 days of pair-feeding with a LS (n = 8) or HS+saline (n = 8) diet. (**D**) Upper panel: GR binding in the cytoplasm (CP), membrane (M), soluble nuclear fraction (SN), chromatin-bound GR (CB), and cytoskeletal (CS) GR in the subcellular fraction in skeletal muscle in mice fed a LS (n = 5) or HS+saline (n = 5) diet. Lower panel: Protein expression of LC3 in its cytosolic form (LC3-I) and as its LC-3-phosphatidylethanolamine conjugate (LC3-II) in the muscle of mice fed a LS (n = 4) or HS+saline (n = 4) diet. (**E**) Quantification of chromatin-bound GR protein expression and ratio of LC3-II/LC3-I protein expression in mice fed a LS (n = 5) or HS+saline (n = 5) diet. (**F**) Plasma corticosterone levels in mice fed a LS (n = 8) or HS+saline (n = 8) diet. (**G**) Relationship between changes (Δ) in body weight and muscle mass, as measured by magnetic resonance lean tissue mass, in mice fed a LS (n = 8) or HS+saline (n = 8) diet. (**H**) In vivo detection of LC3 expression (green) in skeletal muscle of LC3-GFP mice after pair-feeding on a LS or HS+saline diet. Data were determined by multivariate analysis of repeated measurements, by Student's t test for independent samples, or by linear regression.

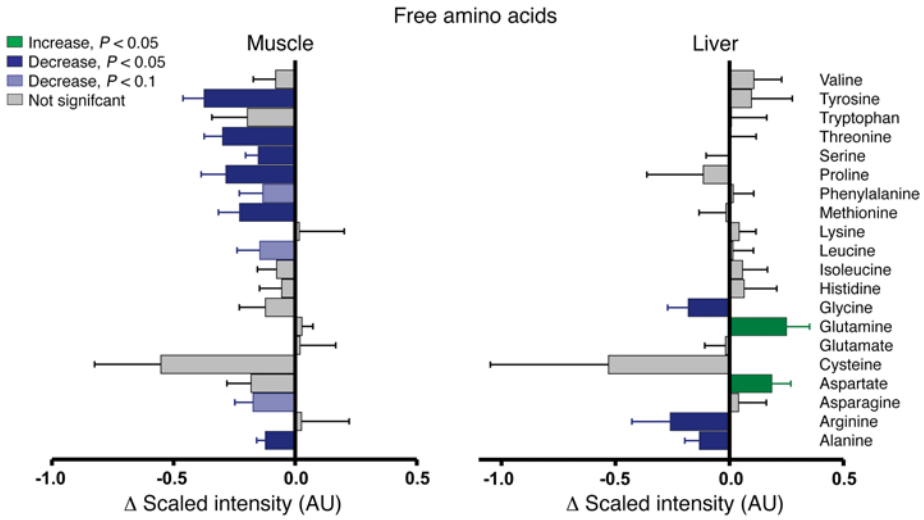

Figure 6. LC-MS/MS free amino acid analysis in skeletal muscle and liver in mice after pair-feeding. Effect of HS+saline on free amino acid levels (reductions in blue; increases in green) after pair-feeding in mice fed a LS (n = 6) or HS+saline (n = 6) diet. Data were analyzed by Student's t test for independent samples.

increased muscle protein breakdown and showed higher corticosterone levels in urine (Table 1) and plasma (Figure 5F). We therefore investigated the relative contribution of muscle mass to body weight loss by nuclear magnetic resonance spectroscopy. Fifty-nine percent of the variability of body weight was explained by changes in lean body mass, which was consistent with salt-induced muscle wasting (Figure 5G). We further confirmed the autophagy component of muscle wasting in vivo in mice expressing GFP under the control of the *LC3* promoter. We found large increases in *LC3* promoter activity in LC3-GFP mice with HS+saline treatment after pair-feeding (Figure 5H). These data support the notion that HS+saline induces a catabolic state for urea osmolyte generation when excess salt is excreted.

Salt promotes nitrogen transfer from muscle to liver. We next hypothesized that muscle protein serves as a nitrogen source for accelerated ureagenesis in HS+saline mice. Metabolomic analysis of free amino acids in skeletal muscle showed a substantial reduction of serine, threonine, methionine, alanine, and tyrosine in HS+saline-treated mice (Figure 6). These amino acids are nitrogen donors for hepatic ureagenesis (Supplemental Figure 8). We found no decrease in free amino acid content in liver. However, liver glutamine and aspartate levels were selectively increased, suggesting a mobilization and redistribution of nitrogen for urea production from muscle to liver.

Arginase utilizes water to convert arginine to urea and ornithine (Supplemental Figures 8 and 9). While increased arginase activity coincided with increased urea levels (Figure 4), ornithine levels were reduced in muscle in HS+saline mice (Figure 7A, left). This finding suggests that other enzyme systems downstream of arginase further converted ornithine, which harbors 2 amino groups. We thus focused on the enzyme ornithine-aminotransferase (OAT) that transfers the C5-amino group from ornithine to 2-oxo-carbon acids, ultimately generating glutamate or proline. Glutamate is the amino source for urea synthesis in the liver. We found a substantial increase in muscle OAT expression in HS+saline mice (Figure 7B, and see Supplemental Figure 10 for the complete, unedited Western blots), but reduced proline levels (Figure 7A, left). These results suggest that the ornithine generated by elevated arginase activity was likely further metabolized to glutamate. Glutamate is not actively transported out of muscle. OAT-initiated provision of muscle nitrogen therefore requires additional transfer of the amino group from glutamate to pyruvate to generate alanine (Supplemental Figure 9). This alanine-glucose-nitrogen shuttle transfers glucose-derived carbon skeletons (pyruvate) and glutamate-derived nitrogen from muscle to liver by way of the transamination to alanine. We found reduced alanine levels (Figure 7A, left), together with unchanged expression of the Na^+/alanine cotransporters SLC38A1 and SLC38A2 (Figure 7B, and see Supplemental Figure 10 for the complete, unedited Western blots) in the muscle of HS+saline mice. In contrast, the expression of SLC38A1 and SLC38A2 was increased in liver (Figure 7B, and see Supplemental Figure 11 for the complete, unedited Western blots), suggesting uptake of muscle alanine in the liver. Urea cycle analysis in liver showed increased arginase activity with increased urea levels (Figure 4) and elevated argininosuccinate levels (Figure 7A, right). The enzyme argininosuccinate lyase converts argininosuccinate to arginine and fumarate (Supplemental Figure 9). We found that liver arginine levels were reduced, presumably as a result of high arginase activity, while fumarate levels were elevated (Figure 7A, right). Despite high fumarate levels, we found no changes in malate or oxaloacetate levels in liver. However, the alternative metabolite aspartate, which ultimately transfers nitrogen from the alanine-glucose-nitrogen shuttle into the urea cycle, was elevated (Figure 7A, right, and Supplemental Figure 9). We interpret these results as indicating that muscle in HS+saline mice increases urea production and transfers nitrogen and glucose via the alanine-glucose-nitrogen shuttle to the liver, where alanine is taken up by increased active transport and preferentially metabolized to urea.

Salt induces ketogenesis, reduces gluconeogenesis, and entails fatty acid oxidation. We next studied the content of glycogen and intermediates for energy metabolism in skeletal muscle and liver (Figure 7A). HS+saline reduced the levels of glucose, glucose-6-phosphate, fructose-6-phosphate, and 6-phosphoguconate in muscle and in liver. The glycogen branch sugars maltotriose, maltotetratose, and maltopentatose were predominantly reduced in the liver. Both muscle and liver showed increased ketone body content. This finding suggests that liver switched pyruvate substrate uti-

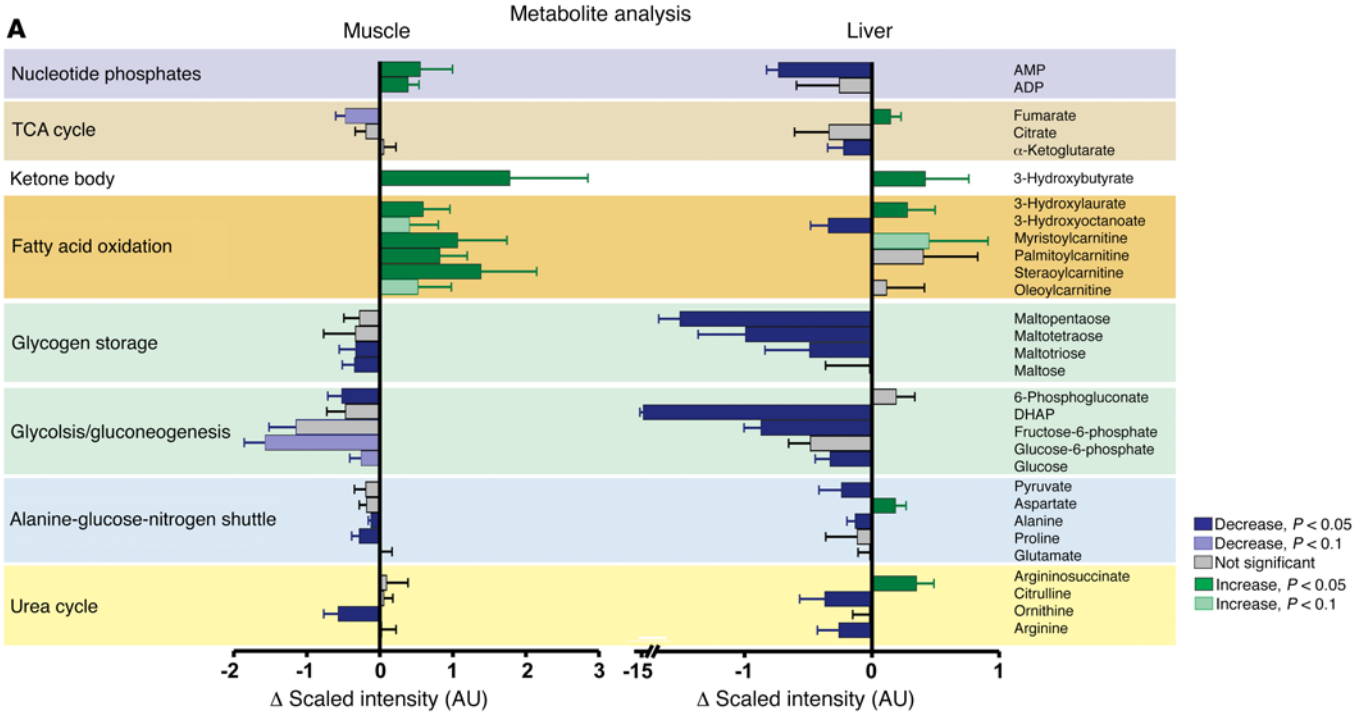
A
Metabolite analysis
Muscle
Liver
Nucleotide phosphates
AMP
ADP
TCA cycle
Fumarate
Citrate
α-Ketoglutarate
Ketone body
3-Hydroxybutyrate
Fatty acid oxidation
3-Hydroxylaurate
3-Hydroxyoctanoate
Myristoylcarnitine
Palmitoylcarnitine
Steraoylcarnitine
Oleoylcarnitine
Glycogen storage
Maltopentaose
Maltotetraose
Maltotriose
Maltose
Glycolsis/gluconeogenesis
6-Phosphogluconate
DHAP
Fructose-6-phosphate
Glucose-6-phosphate
Glucose
Alanine-glucose-nitrogen shuttle
Pyruvate
Aspartate
Alanine
Proline
Glutamate
Urea cycle
Argininosuccinate
Citrulline
Ornithine
Arginine
Decrease, P < 0.05
Decrease, P < 0.1
Not significant
Increase, P < 0.05
Increase, P < 0.1
-2 -1 0 1 2 3
Δ Scaled intensity (AU)
-15 -1 0 1
Δ Scaled intensity (AU)

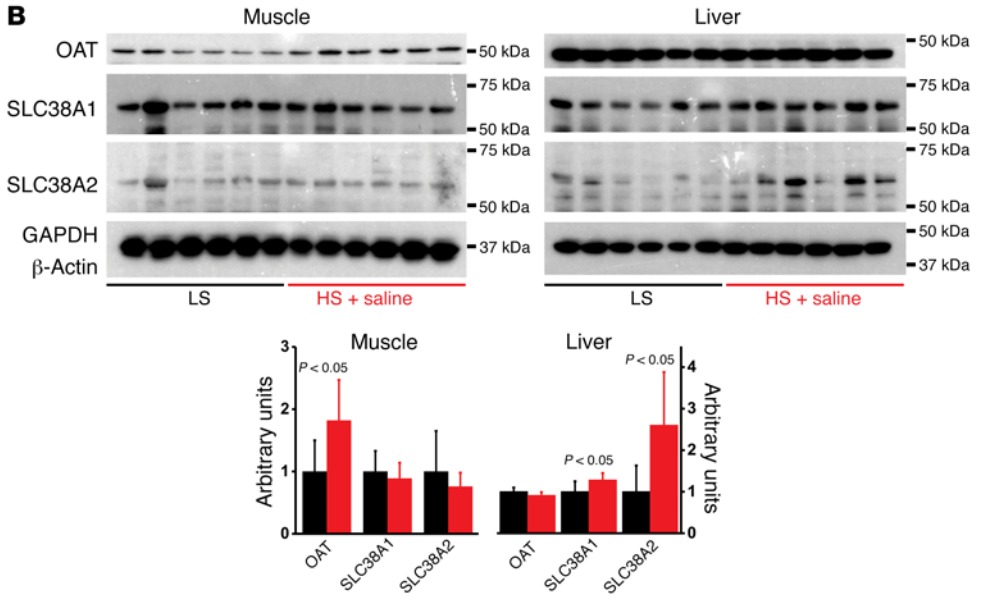
B
Muscle
Liver
OAT
SLC38A1
SLC38A2
GAPDH
β-Actin
50 kDa
75 kDa
37 kDa
LS
HS + saline
Muscle
Liver
Arbitrary units
P < 0.05
OAT
SLC38A1
SLC38A2

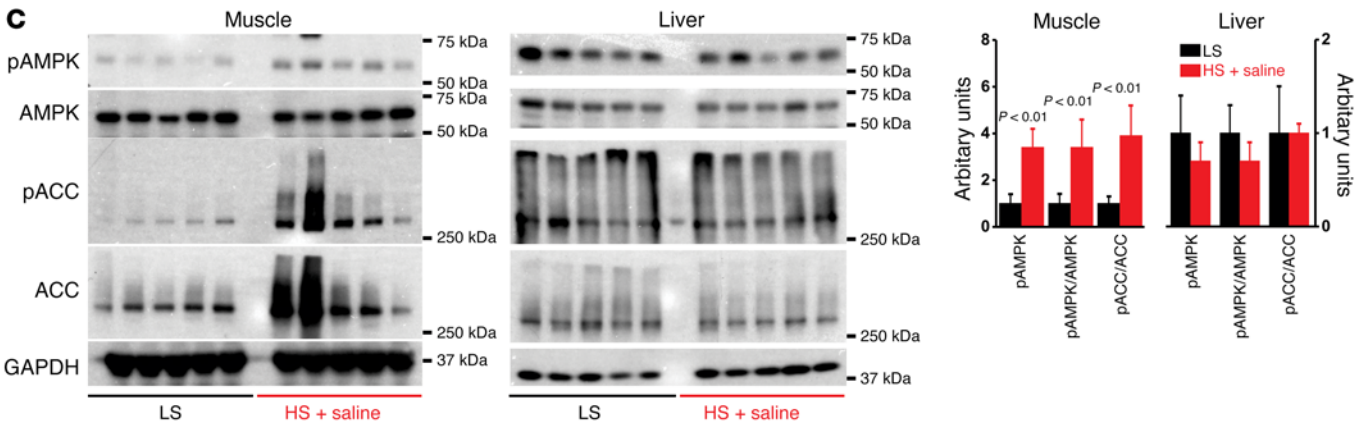
C
Muscle
Liver
pAMPK
AMPK
pACC
ACC
GAPDH
75 kDa
50 kDa
250 kDa
37 kDa
LS
HS + saline
Muscle
Liver
LS
HS + saline
Arbitrary units
P < 0.01
pAMPK
pAMPK/AMPK
pACC/ACC

Figure 7. LC-MS/MS metabolite analysis in liver and skeletal muscle of mice after pair-feeding. (**A**) Effect on key metabolites of energy metabolism (AMP and ADP), the TCA cycle, ketone body formation, fatty acid oxidation, glycogen storage, glycolysis/gluconeogenesis, the alanine-glucose-nitrogen shuttle, and the urea cycle in muscle and liver in pair-fed mice given a LS (n = 6) or HS+saline (n = 6) diet (reductions in blue; increases in green). (**B**) Protein expression of OAT and the Na^+-alanine cotransporters SLC38A1 and SLC38A2 in the same mice. (**C**) Protein expression of phosphorylated and unphosphorylated AMPK ACC in the same mice. Expression of GAPDH (37 kDa) and β-actin (42 kDa) proteins served as a loading control. Data were analyzed by Student's t test for independent samples.

lization from energy-intense gluconeogenesis to energy-neutral ketogenesis and thereby reprioritized its energy expenditure in favor of urea osmolyte production (Supplemental Figure 12).

Liver ketogenesis deprives muscle of glucose. Muscle in HS+saline mice showed increased fatty acid carnitine esters and their respective 3-hydroxy isoforms (Figure 7A). This finding, corroborated by the observed RQ reduction (Figure 5A), indicates preferential mitochondrial β-oxidation in HS+saline mice. We conclude that muscle in HS-saline mice utilized ketone bodies together with fatty acids as energy fuels, while the availability of glucose was reduced.

However, the reduced availability of glucose also reduces glycolytic pyruvate generation (Supplemental Figure 12). Pyruvate is an essential substrate that initiates nitrogen transfer from muscle to liver via the alanine-glucose-nitrogen shuttle (Supplemental Figure 9). Liver-driven glucose/pyruvate deprivation may therefore explain the autophagy and muscle protein breakdown observed in HS+saline mice, because muscle protein remained the major available source of glutamate and pyruvate.

Energetic consequences of salt in muscle and liver. In line with the catabolic nature of urea production and nitrogen mobilization in muscle, we found increased AMP and ADP levels in skeletal muscle in HS+saline mice (Figure 7A, left). AMPK, which acts as a sensor of cellular energy status, is considered a key enzyme in conditions of cellular energy deficit. AMPK is able to inhibit metabolic pathways that consume energy and increases mechanisms that produce energy (5). Binding of AMP to AMPK inhibits dephosphorylation of the kinase (6, 7). Phosphorylated AMPK (p-AMPK) facilitates fatty acid oxidation in mitochondria (8) and promotes autophagy in skeletal muscle (9, 10). HS+saline mice with increased AMP levels in muscle showed increased p-AMPK protein and an increased p-AMPK/AMPK ratio (Figure 7C, and see Supplemental Figure 13 for the complete, unedited Western blots). p-AMPK promotes mitochondrial fatty acid oxidation (11, 12) by phosphorylation of its downstream target acetyl CoA carboxylase (ACC). ACC promotes carboxylation of acetyl CoA to generate malonyl-CoA and initiate fat storage (13). p-AMPK–driven phosphorylation of ACC inhibits its carboxylase activity and thereby promotes mitochondrial β-oxidation (14). We found that HS+saline increased p-ACC levels and the p-ACC/ACC ratio (Figure 7C, and see Supplemental Figure 13 for the complete, unedited Western blots). These results indicate that a HS diet leads to an energy deficit in skeletal muscle, which induces an AMP-driven increase of fatty acid oxidation by p-AMPK–mediated phosphorylation of ACC.

In contrast to muscle, liver in HS+saline mice showed reduced AMP levels (Figure 7A, right), suggesting no organ-specific energy deficit, despite massively increased urea production and reduced availability of glucose or glycogen fuels. In line with low AMP levels, p-AMPK and p-ACC were not elevated in the liver of HS+saline mice (Figure 7C). We interpret these results as indicating that reduced gluconeogenesis and a switch to ketogenesis (Supplemental Figure 12) help prevent an energy deficit in liver, despite the energy-intense urea osmolyte generation that occurs in catabolic HS+saline mice.

Salt decreases cardiovascular energy expenditure. The observed reprioritization of energy metabolism in our HS+saline mice represents a typical adaptation pattern for water conservation in organisms, termed aestivation (15). In aestivators, the energy-intense nature of urea osmolyte generation for body water conservation also includes reduced cardiovascular energy expenditure (16). We therefore hypothesized that HS+saline not only reprioritized energy metabolism, but also induced reduced cardiovascular energy expenditure in mice. We therefore used radiotelemetry to study the cardiovascular response to our 4 different salt-intake regimens in 6 mice (Figure 8). The diet consisting of 4% NaCl chow with tap water increased systolic BP (SBP) from 119 ± 13 mmHg to 124 ± 11 mmHg ($P < 0.05$), without significant changes in heart rate (Figure 8A). Replacement of water with isotonic saline (HS+saline diet) not only led to a catabolic state with reprioritization of urea osmolyte and energy metabolism (Figures 5–7), but also induced the expected changes in cardiovascular energy expenditure. The initial response to HS+saline exposure was characterized by a steep increase in heart rate, with a monophasic short R-R interval distribution pattern (Figure 8B), and an increase in locomotor activity, suggesting an alarm reaction with predominant sympathetic drive. Within 4 days of HS+saline treatment, mice had markedly lower heart rates that were even below the initial baseline rate and now showed a biphasic distribution of short and prolonged R-R intervals, consistent with high parasympathetic tone (Figure 8B). SBP levels were intimately coupled with the cardiovascular energy expenditure level. Thirty-two percent of the variability in SBP was explained by changes in heart rate, suggesting that cardiovascular energy expenditure and sympathetic nerve drive during activity and inactivity were important determinants of the salt-induced elevation and reduction in BP (Figure 8C). Additional pair-feeding not only induced total body energy deficit and catabolism (Figures 5–7), but also resulted in a robust reduction in cardiovascular energy expenditure, with a low heart rate, low BP, and low locomotor activity, despite massive salt intake. Finally, we tested the hypothesis that the initial BP increase we observed in HS+saline-fed animals was inducible by an acute stressor. We found that intra-arterial BP was significantly elevated in mice fed a HS+saline diet for 2 consecutive weeks when we measured BP acutely in restrained animals (Figure 8D). We interpret these findings as indicating that HS+saline not only leads to catabolic urea production with reprioritization of energy metabolism, but also induces a reduction in cardiovascular energy expenditure with a reduced heart rate and low BP. This negative energy balance–driven cardiovascular response in HS+saline mice was rapidly reversible during acute alarm responses triggered by an external stressor. We conclude that the metabolic and cardio-

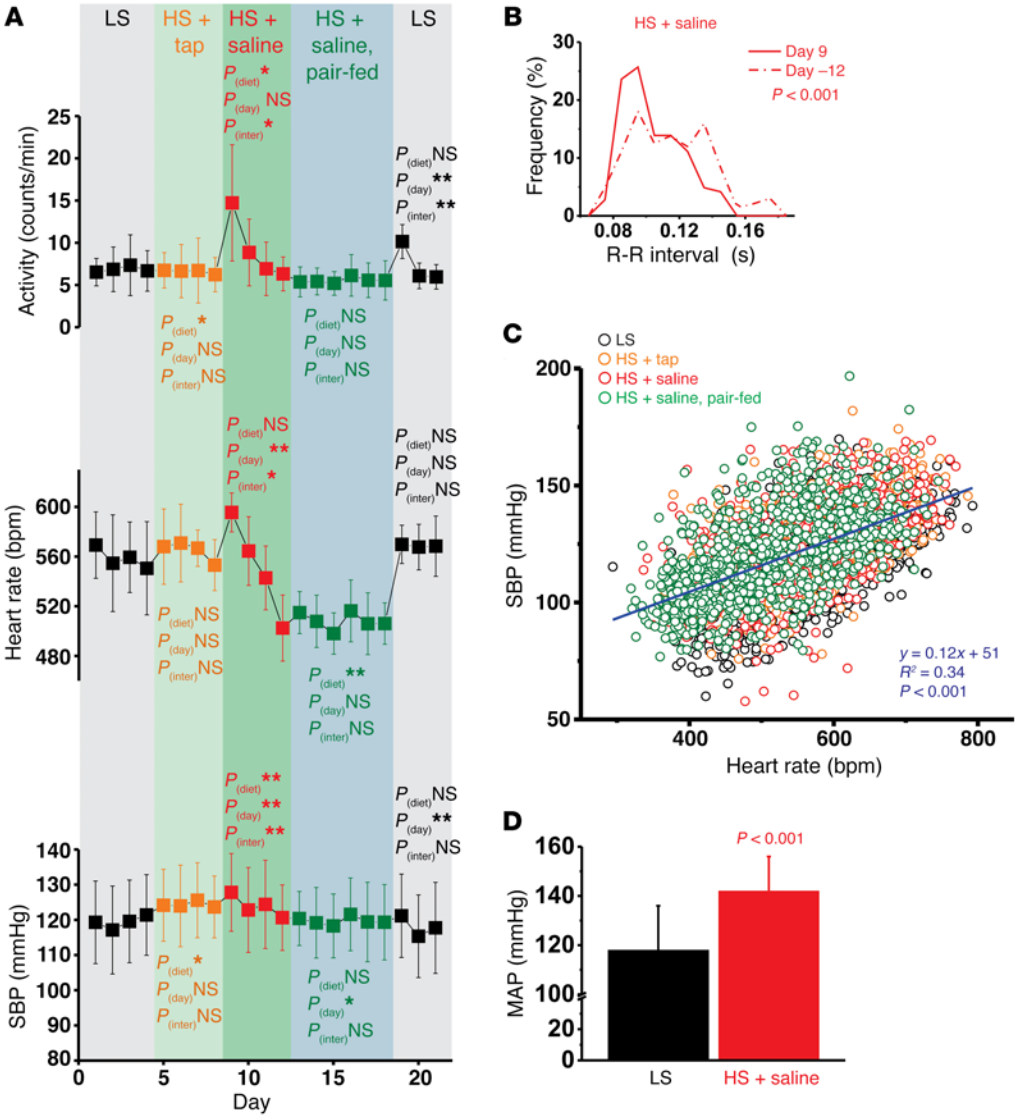

Figure 8. Cardiovascular responses to dietary salt loading. Dietary salt levels were as follows: black = LS diet; orange = 4% NaCl diet with tap water (HS+tap); red = 4% NaCl diet with additional isotonic saline (HS+saline); green = 4% NaCl diet with isotonic saline and calorie intake restriction (HS+saline, pair-fed). (**A**) Locomotor activity, heart rate, and SBP in 6 mice over a 21-day period. (**B**) R-R interval distribution in the same mice after 1 (Day 9) and 4 (Day 12) days of a 4% NaCl diet with isotonic saline. (**C**) Relationship between heart rate (bpm) and SBP (mmHg) in the same mice. (**D**) Mean arterial BP (MAP) in acutely restrained mice that were fed a LS (n = 20) or HS+saline (n = 18) diet ad libitum for 2 weeks. $^*P < 0.05$ and $^{**}P < 0.01$. $P_{(diet)}$: effect of dietary intervention versus LS level; $P_{(day)}$: effect of intervention day; $P_{(inter)}$: interaction between dietary intervention and day of intervention. Data were determined by multivariate analysis of repeated measurements, Student's t test for paired samples, Student's t test for independent samples, and by linear regression.

vascular response to HS+saline we observed in our mice is typical for water conservation by aestivation.

Discussion

Our major finding is that the excretion of surplus dietary salt is not confined to parallel osmolyte and water movement into the urine to induce osmotic diuresis and reduce the extracellular volume. Instead, we show that the body's response to dietary salt additionally relies on the maintenance of negative FWC and urea accumulation in the kidneys, while Na^+ and accompanying anions are concentrated in the urine (Supplemental Figure 14). Our findings suggest that the kidneys, liver, and skeletal muscle form a physiological-regulatory network for extracellular volume control by coupling salt-dominated osmolyte excretion with antiparallel, urea-dominated water conservation when salt intake is high.

Water conservation by reprioritization of renal osmolyte transport in response to dietary salt. The natriuretic concept of extracellular volume control suggests that the body excretes Na^+ in an effort to reduce the extracellular volume (1, 17). In expanding this concept, we suggest that the extracellular volume is controlled by natriuretic-ureotelic regulation. The water-saving principle of the urine concentration process by renal medullary urea accumulation was established earlier (18) and has been confirmed in mice with targeted disruption of the renal urea transporters (19, 20). In line with earlier findings indicating that urea and NaCl osmolytes exert opposing effects on UT-A1–driven urea transport during acute osmotic diuresis (21), we show here that this urea-dependent water conservation principle is utilized to maintain the renal concentration process and thereby possibly counterbalance the osmotic-diuretic effect of salt excretion. The resulting endogenous water accrual allows constancy in urine volume formation, despite massive natriuresis. The reduced dependency on external water sources can be viewed as an advantageous physiological principle for body water control. Endogenous water accrual within the renal concentration mechanism is not restricted to mice under extreme salt-intake conditions, but occurs with increasing Na^+, K^+, or urea osmolyte excretion in mice and humans across all levels of salt intake (Figure 1, C and D). Bankir and Yang noted earlier that the excretion of dietary salt during the Dietary Approaches to Stop Hypertension (DASH) sodium trial increased the Na^+

concentration in the subjects' urine, without increasing the urine volume (22). The findings suggest that urine concentration, and therefore regulation of water conservation, is an important control system for urine formation and extracellular volume homeostasis in humans and mice with high salt intake.

Water conservation by reprioritization of urea osmolyte production in response to dietary salt. The ultimate need to keep water in the body when salt osmolytes are excreted not only requires renal urea recycling, but also necessitates hepato-muscular urea osmolyte generation in HS+saline mice. We show how kidney, liver, and muscle urea content explains 87% of the variability in plasma urea content in mice, with liver explaining most of the variability and muscle explaining the least (Figure 4). Increased arginase activity in liver and muscle, but not kidney, explains 70% of the variability in plasma urea levels. This finding indicates that renal transport of urea osmolyte and urea osmolyte production in liver and skeletal muscle are integrated physiological-regulatory components. Pharmacological arginase inhibition prevented the salt-driven increase in tissue urea content and reduced plasma urea concentrations in HS+saline mice. These findings suggest a hepato-renal-musculoskeletal regulation of extracellular water conservation by osmolyte production in liver and muscle and by urea osmolyte recycling in the kidney. Given the energy-consumptive nature of urea osmolyte generation, perpetuation of this urea-dependent water conservation process has major consequences on energy metabolism when salt intake remains high.

Water conservation by reprioritization of energy expenditure in response to dietary salt. We have studied the salt-induced reprioritization of energy expenditure for urea-driven water conservation in liver, skeletal muscle, and the cardiovascular system. Liver urea production is energy intense (Supplemental Figure 12). Liver uses the glucose-alanine cycle to transfer the nitrogen necessary for urea production into the hepatic urea cycle. This transamination pathway is also known for the transfer of muscle pyruvate/amino acid from muscle to liver for gluconeogenesis during starvation (23–25). During energy surplus, liver thus invests energy to generate urea from amino acid–derived nitrogen and to generate glucose from pyruvate. Catabolic HS+saline mice economized energy expenditure into the glucose-alanine cycle by reprioritizing liver metabolism. HS+saline mice had increased energy-intense urea osmolyte generation in the liver, while showing restricted energy expenditure for glucose generation by switching hepatic pyruvate substrate metabolism from energy-intense gluconeogenesis to energy-neutral ketogenesis. We interpret this finding as showing that HS+saline mice reprioritized their liver energy metabolism to ensure urea-driven water conservation. The large increase in hepatic osmolyte production occurred at the expense of ketogenesis to prevent a hepatic energy deficit and organ dysfunction.

In contrast to liver, skeletal muscle metabolism in HS+saline-fed mice was characterized by catabolic substrate and fuel exploitation with extrahepatic urea generation (Figure 4), glucocorticoid receptor activation, muscle protein breakdown and autophagy (Figure 5), exploitation of muscle amino acids (Figure 6), and provision of muscle nitrogen and pyruvate via the alanine-glucose-nitrogen shuttle for urea production and ketogenesis in the liver (Figure 7). The resulting fuel deficit led to a negative energy balance, which mechanistically promoted p-AMPK/p-ACC–driven fatty acid oxidation (Figure 7). This finding suggests that skeletal muscle showed increased metabolic water production in HS+saline-fed mice. Furthermore, HS+saline induced a quantifiable reduction in lean body mass in the animals as soon as an increase in food intake, to compensate for the salt-driven catabolic state, was not permitted during pair-feeding (Figure 5).

We focused on the change in body fluid and body mass composition that occurs with muscle mass loss (Supplemental Figure 15). Independently of glucocorticoid-driven changes in metabolism, LS mice, HS+tap mice, and HS+saline mice accrued approximately 80% of their estimated extracellular volume by negative FWC within the renal concentration mechanism. Additional glucocorticoid-driven catabolism in HS+saline diet–fed mice resulted in a lean body mass loss of 2.5 g, which had a water content of 0.7 ml/g. Thus, the mice must have released 1.8 ml of water stored in skeletal muscle cells into the extracellular space, which corresponds to approximately 35% of the estimated normal size of the extracellular volume. In HS+tap diet–fed mice, natriuretic-ureotelic regulation of salt excretion was limited to renal free water accrual by maintenance of the renal concentration mechanism.

The switch from gluconeogenesis to ketogenesis we observed in the liver in HS+saline mice represents a hypometabolic response that reduces metabolic energy expenditure for glucose formation and preferentially produces urea osmolytes for body water conservation. HS+saline-fed mice showed a similar reduction in cardiovascular energy expenditure, with a reduced heart rate and low BP. The BP reduction in HS+saline mice was immediately reversible when the animals were exposed to an acute stressor (Figure 8).

Aestivation as an alternative pathophysiological feature of high salt intake. The unifying hypothesis to explain the above-mentioned phenotype of increased renal urea recycling, increased urea production in liver and skeletal muscle, and reprioritization of liver, muscle, and cardiovascular energy expenditure is that the HS diet without free access to water induced aestivation in our mice. Life under arid conditions often restricts water availability, especially in the heat, which is a common trigger for aestivation (aestas: summer) (15). Aestivation can be summarized as a variety of physiological self-preservation strategies to prevent dehydration and death. The main underlying motif of aestivation success is the conservation of body water. The need to conserve body water when salt intake is high apparently induces an aestivation-like phenotype in mice.

Homer Smith first studied osmolyte-driven control over body hydration in aestivating lungfish (26). Restricted to subterranean mud cocoons, lungfish aestivate when surrounded by water that is hyperosmolal compared with their body fluids, predisposing the fish to body water loss. To prevent dehydration, aestivating lungfish increase their urea content in both plasma and tissue (27, 28). Like our HS+saline mice, aestivating lungfish induce energy-intensive urea production in the liver (29, 30) and exploit muscle protein as a nitrogen source (26). The resulting energy deficit leads to reprioritization of energy metabolism during aestivation. Also similar to our HS+saline mice, snails aestivating in the heat show increased p-AMPK activity in foot muscle (31), including phosphorylation of ACC with inhibition of lipogenesis and glycogen synthesis, resulting in exploitation of available fuels. We additionally showed that liver in HS+saline mice reduced glucogene-

sis and increased ketogenesis, thereby preventing simultaneous energy-intense glucose and urea generation. Finally, and also similar to our HS+saline mice, aestivating catabolic lungfish undergo a reduction of their heart rate and BP in an effort to reduce their energy deficit (16, 32). However, and in contrast to hibernation (33), aestivation is characterized by fairly light dormancy involving no physiological changes that cannot be very rapidly reversed (15). In line with this finding, the HS+saline-fed mice in our study rapidly switched to the typical salt-sensitive hypertension BP phenotype during acute stress. The elevated corticosterone levels observed in our HS+saline mice may facilitate such acute stress reactions. The similarities between aestivators and our HS+saline mice demonstrate that the body's response to high dietary salt consumption includes a reprioritization of body's metabolism and energy expenditure to ensure sufficient urea osmolyte production and thereby prevent dehydration.

Limitations. Mice are an imperfect research model for simulating metabolic changes in humans. Normalized for body mass, normal fluid intake in our healthy mice on a salt-free diet would correspond to 18 l/d water intake in an 80-kg human and be considered a disease state. Across all diets, water conservation by negative FWC within the renal concentration mechanism was 16-fold higher in our mouse water balance studies compared with our human water balance studies. Normal food consumption in mice corresponded to 12 kg/d food intake in an 80-kg human and resulted in a predominance of urea osmolyte excretion compared with that detected in the human subjects. Even a 4% NaCl chow diet did not reduce this predominant urea excretion to the levels observed in humans. Finally, a 6-g/d increase in salt intake without free water restriction increased cortisol levels in humans. Comparable salt diet–driven increases in corticosterone levels, coupled with the induction of a catabolic state, were only found with the 4% NaCl chow diet in combination with isotonic saline water for drinking. Combining a 4% NaCl chow diet with free access to water neither increased glucocorticoid levels nor induced a catabolic state in mice. We can only speculate that nonrodent models would require less massive salt loading and free water restriction to study salt-driven catabolism experimentally.

Summary and perspective. We conclude that the biological signature of renal surplus osmolyte excretion in mice and humans is endogenous free water accrual and, thus, physiological conservation of body water. Key in the physiological response to dietary salt we observed was the maintenance of the urine concentration mechanism. The renal medulla is a physiological barrier designed to excrete surplus osmolytes and to conserve filtrated water by tubular reabsorption. Excess intake of dietary salt challenges this barrier principle, because the subsequent excess salt excretion can induce osmotic diuresis and predisposes the organism to water loss. HS+tap water–fed mice and HS+saline-fed mice therefore strengthened the osmotic force of their renal barrier by urea transporter–driven urea recycling for renal water conservation. Besides renal urea osmolyte conservation, natriuretic-ureotelic regulation additionally included a catabolic hormone profile with hepatic and extrahepatic urea osmolyte production in HS+saline mice. The energy-intense nature of urea osmolyte production couples urea-driven water conservation with the adverse effects of reprioritization of energy expenditure, which results in an aestivation-like phenotype. Disease states with a predisposition to extracellular volume contraction therefore may be characterized by increased energy uptake, catabolic exploitation of endogenous nitrogen and energy fuels, and reprioritization of energy expenditure in favor of alternative osmolyte production for body water conservation.

Methods

Animal experiments. After a 1-week acclimatization, during which the animals had unlimited access to tap water and regular chow (5LOD; PMI Nutrition International), as provided by our animal facility, we fed 8- to 10-week-old male C57/B6J mice (The Jackson Laboratory) a LS diet (<0.1% NaCl; TD90228; Harlan Laboratories) (Supplemental Table 1) with tap water (LS); a HS diet (4% NaCl; TD92034; Harlan Laboratories) (Supplemental Table 1) with tap water (HS+tap); or a HS diet with 0.9% saline to drink (HS+saline) for 4 consecutive weeks and then pair-fed the animals for 2 weeks to match energy intake in the HS and LS groups. In a separate experiment, we studied the effect of additional arginase inhibition with 40 mg/kg/d i.p. injection of NOHA (Bachem) in 3 experimental groups (group 1: LS; group 2: HS+saline; group 3: HS+saline+NOHA). These mice were also fed ad libitum for 4 weeks, followed by 2 weeks of pair-feeding. Six weeks after the beginning of the LS or HS treatment, the mice were euthanized, and blood and tissue samples were collected.

Pair-feeding. Mice were allowed ad libitum access to the specified diet for 4 weeks, followed by 2 weeks of pair-feeding. Fluid intake was not restricted. During the pair-feeding stage of the experiment, each individual animal from the HS group was administered the amount of a HS diet equal to the average amount of chow the LS group had consumed the day before.

Urine collection. Two weeks into the LS, HS+tap, or HS+saline treatment, the mice were placed into metabolic cages (Hatteras Instruments) for 20 hours without access to food. LS- and HS+tap-treated mice received tap water, and HS+saline-treated mice received 0.9% saline to drink during the period of urine collection. To test the relationship between food and fluid intake of the previous day and osmolyte and water excretion in the metabolic cage, we additionally measured food and fluid in the normal cages 24 hours before the mice were transferred into the metabolic cages.

Electrolyte and osmolality measurements. Sodium and potassium concentrations in plasma and urine were measured by flame photometry (EFOX5053; Eppendorf). Plasma and urine osmolality were measured by vapor pressure osmometry (Wescor). FWC in the balance studies was calculated as follows: urine volume × (1 – urine osmolality/plasma osmolality), taken from measured urine volume, measured urine osmolality, and an estimated constant plasma osmolality of 300 mOsm/kg.

Urea and arginase activity. Tissue was homogenized in protein extraction reagent (Thermo Fisher Scientific) with an added proteinase inhibitor cocktail (Roche), and an Omni TH homogenizer was used immediately after tissue collection. After homogenization, the samples were centrifuged at 13,000 ×*g* for 20 minutes. To extract urea from protein samples, the samples were filtered using a 10-kDa molecular weight cutoff spin column (EMD Millipore). The urea-depleted supernatant was used for arginase activity determination, and tissue urea content was measured with the diluent. Urea concentration was measured in plasma, urine, and tissue by colorimetry using a BioVision urea assay kit. Tissue arginase activity was measured using an arginase assay kit (Sigma-Aldrich). Tissue arginase catalyzes the con-

version of added arginine to urea and ornithine. One unit of arginase is the amount of enzyme that converts 1 mmol L-arginine to ornithine and urea per minute at pH 9.5 and 37°C.

Western blot analysis. We quantified protein expression in liver and muscle by Western blotting. Protein was extracted as described above. Tissue protein (20–30 μg/lane) was size separated by SDS-PAGE on 8% to 16% gradient gels and then electroblotted onto PVDF membranes (EMD Millipore). We used the following commercially available primary antibodies: rabbit polyclonal anti-ornithine aminotransferase antibody (1:1,000; Abcam; ab137679); mouse monoclonal anti-SLC38A1 antibody (1:1,000; Abcam; ab134268); rabbit polyclonal anti-SLC38A2 antibody (1:1,000; Abcam; ab90677); rabbit polyclonal anti-LC3 antibody (1:1,000; Cell Signaling Technology; 2775); rabbit polyclonal anti-p62 antibody (1:1,000; Cell Signaling Technology; 5114); rabbit monoclonal anti-atg5 antibody (1:1,000; Cell Signaling Technology; 12994); rabbit polyclonal anti–p–acetyl-CoA carboxylase (Ser79) antibody (1:1,000; Cell Signaling Technology; 3661); rabbit polyclonal anti–acetyl-CoA carboxylase antibody (1:1,000; Cell Signaling Technology; 3622); rabbit polyclonal anti–p-AMPKα (Thr172) antibody (1:1,000; Cell Signaling Technology; 4188); rabbit polyclonal anti-AMPKα antibody (1:1,000; Cell Signaling Technology; 1532); and HRP-conjugated anti–β-actin (1:10,000; Sigma-Aldrich; A3854) or anti-GAPDH antibody (1:10,000; Sigma-Aldrich; G9295). Blots were washed and then incubated with an HRP-conjugated secondary antibody (1:5,000; Santa Cruz Biotechnology Inc.; sc2004) before being subjected to densitometric analysis. For urea transporter protein expression, we first dissected inner and outer medullas from the mouse kidney. The tissues then were placed into ice-cold isolation buffer (10 mM triethanolamine, 250 mM sucrose, pH 7.6, 1 μg/ml leupeptin, and 2 mg/ml PMSF) and homogenized, and SDS was added to a final concentration of 1%. Samples were diluted with Laemmli sample buffer to a final protein concentration of 1 mg/ml and boiled for 1 to 3 minutes. Proteins were separated by PAGE. UT-A1 (25 μg/lane) was separated on a 10% gel, then proteins were electroblotted to PVDF membranes (EMD Millipore). Blots were incubated with our antibody to the C-terminus of UT-A1 and UT-A2 (34). Alexa Fluor 680–linked anti-rabbit IgG (Thermo Fisher Scientific) was used as the secondary antibody. Then, the secondary antibody was visualized and densities analyzed with the Odyssey protein analysis system (LI-COR Biosciences).

Corticosterone measurements. Corticosterone levels in plasma and urine were determined simultaneously using liquid chromatography–tandem mass spectrometry (LC–MS/MS). Detection was achieved by atmospheric pressure chemical ionization in positive ion mode with multiple reaction monitoring for the transitions (qualifier transition: *m/z* 347.2/121.2 [347.2/91.1]) for corticosterone and 355.2/125.2 for corticosterone-d8 (internal standard). One hundred microliters of serum (10 μl urine) was deproteinized with methanol/zinc sulphate (50 g/l, 1/1 v/v). After centrifugation, the supernatants were applied to an online solid-phase extraction column with subsequent high-pressure liquid chromatographic separation. The intra-assay variation coefficient was 1.3%–11% for corticosterone (concentration range, 3–368 ng/ml).

Indirect calorimetry. To detect a catabolic state with increased fatty acid oxidation in vivo, oxygen consumption (VO_2) and carbon dioxide production (VCO_2) were continuously measured in 8 LS-treated and 8 HS-treated mice during our experiments using an Oxymax Indirect Calorimetry System (Columbus Instruments). Mice stayed individually in the calorimetry system for 1 week. The RQ was calculated as VCO_2/VO_2.

Metabolomic profile analysis. Liquid nitrogen snap-frozen liver and muscle samples from 6 LS- and 6 HS+saline-treated mice were aliquoted and used for detection and relative quantification of metabolites by Metabolon as previously described (35). All metabolites except for urea were measured by ultra-high-performance LC-MS/MS (UPLC-MS/MS) (Metabolyn; Metabolon Inc.). We studied key metabolic components of glucose, amino acid, fatty acid, and urea metabolism. Salt-induced differences in the scaled intensity of the metabolites are reported (Δ scaled intensity, Figures 5 and 6).

Subcellular GR protein expression in skeletal muscle. Muscular tissue samples were separated into cytoplasmic (CP), membrane (M), soluble nuclear fraction (SN), chromatin-bound (CB), and cytoskeletal (CS) protein extracts using a subcellular protein fractionation kit for tissues (Thermo Fisher Scientific). Subcellular GR expression was quantified from these subcellular muscle protein lysates by Western blotting. Proteins (20 μg/lane) were size separated by SDS-PAGE on 8% to 16% gradient gels and then electroblotted onto PVDF membranes (EMD Millipore). A rabbit polyclonal antibody against the GR (1:500; Santa Cruz Biotechnology Inc.; sc1004) and an HRP-conjugated anti-rabbit secondary antibody (1:5,000; Santa Cruz Biotechnology Inc.; sc2004) were used for Western blot analysis. We calculated subcellular GR expression levels as the percentage of total GR expression for each sample.

Body composition measurement. Body composition (fat mass, lean mass, and free fluid) was determined using a mq10 nuclear magnetic resonance analyzer (Minispec ND2110; Bruker) immediately before and 2 weeks after pair-feeding.

In vivo autophagy detection in the skeletal muscle. GFP-LC3#53 reporter mice with GFP expression under the control of the *LC3* promoter were obtained from the Riken BioResource Center (Kyoto, Japan) (36). The skeletal muscle from a right hind limb was perfused with PBS and 4% paraformaldehyde and then fixed in 4% paraformaldehyde for 4 hours at room temperature. The skeletal muscle was sectioned (>100-μm thickness) and incubated with a 20% sucrose solution for 30 minutes. A rabbit anti-GFP antibody (Thermo Fisher Scientific) was used as the primary antibody. The capillary bed and nuclei were stained with Alexa 594–conjugated isolectin B4 and DAPI, respectively. The sections (10- to 50-μm thickness) were observed by 2-photon microscopy (FV1000-MPE; Olympus).

BP, heart rate, and locomotor activity. BP, heart rate, and locomotor activity were monitored in 6 mice during the experiment using an implantable telemetry system (Data Sciences International). Mice were anesthetized with an i.p. injection of ketamine-xylazine. After isolation of the left common carotid artery, the catheter connected to the transducer was introduced into the carotid artery and advanced until the tip was just inside the thoracic aorta. The transmitter was positioned along the right flank, close to the hind limb. Two weeks after recovery, BP, heart rate, and activity measurements were started. We additionally measured BP via an arterial line in acutely restrained mice (129/Sv background) following a 2-week LS diet (n = 20) or HS+saline diet (n = 18), as reported previously (37).

Statistics. All data are expressed as the mean ± SD. Differences in metabolite expression, urea content, arginase activity, Western blot results, plasma and urine osmolytes, corticosterone levels, body weight, lean body mass, and BP in response to experimental salt load-

ing were analyzed by 2-tailed Student's *t* test for unpaired samples or by the general linear model for independent samples, followed by post-hoc testing using Bonferroni's algorithm. The time course of the changes in food intake, body weight, respiratory coefficient, and telemetric readout of locomotor activity, heart rate, R-R interval, and BP was analyzed using the general linear model for repeated measurements to test for the effect of diet and time and their interaction (day × diet). A *P* value of less than 0.05 was considered statistically significant. SPSS software, version 20.0 (SPSS Inc.) was used for statistical analysis.

Study approval. Water balance in 10 human subjects was studied during a simulated space flight to Mars. The study was conducted at the Institute for Biomedical Problems in Moscow and approved by the Russian National Committee on Bioethics of the Russian Academy of Sciences. Details on the subjects and their environmental conditions, dietary salt intervention, and experimental procedures are presented in the accompanying article (4). The IACUC of Vanderbilt University approved all experiments, and mice were housed and cared for in accordance with the *Guide for the Care and Use of Laboratory Animals* (National Academies Press, 2011).

Author contributions

KK, SD, YZ, TP, JDK, JMS, DN, AN, LL, DHW, SID, and JT performed the animal experiments. PN, AS, NR, JJ, and DNM provided essential material and contributed to the design of the experiments. JDK, LML, and JMS analyzed UT-A expression and interpreted the data. DN and AN performed the experiments with LC3-GFP mice and analyzed the data. KK, SID, and AED performed the arginase assay experiments. YZ, LML, DHW, and JT designed and performed the metabolic in vivo studies and interpreted the data. DGH performed the telemetry measurements. MR performed the corticosterone measurements and analyzed the data. KK, SD, and JT designed and planned the experiments and analyzed and interpreted data. KK, SD, AM, RCH, FCL, and JT wrote the manuscript. JT designed and supervised the research project.

Acknowledgments

This work was supported by grants from the NIH (RO1 HL118579-01, to JT; R01-DK41707 and R01-DK89828, to JS; and U24 DK059637, to DHW); the American Heart Association (AHA) (14SFRN20770008); the German Federal Ministry for Economics and Technology/DLR Forschung unter Weltraumbedingungen (50WB1624, to JT); the Deutsche Forschungsgemeinschaft (DFG) (SFB 643 B16, to JT and JJ; DA 1835/1-1, to SD); the TOYOBO Biotechnology Foundation (to KK); and the Interdisciplinary Center for Clinical Research Erlangen (to JT). We thank N. Mizushima (University of Tokyo) for providing GFP-LC3#53 mice. We are grateful to the excellent technical assistance of Yan Zhao (Vanderbilt University Medical Center, Nashville, TN, USA), Jenny Hähnel, and Ulrike Goller (University Clinic Erlangen, Erlangen, Germany).

Address correspondence to: Jens Titze, Division of Clinical Pharmacology, Vanderbilt University Medical Center, 2213 Garland Avenue, P435F MRBIV, Nashville, Tennessee 37232, USA. Phone: 615.343.1401; E-mail: jens.m.titze@vanderbilt.edu.

1. Pitts RF. *Physiology of the Kidney and Body Fluids: An Introductory Text*. Chicago, Illinois: Year Book Medical Publishers; 1974:11–34.
2. Rose BD. In: Rose BD ed. *Clinical physiology of acid-base and electrolyte disorders*. New York, New York: McGraw-Hill, Inc.; 1994:235–260.
3. Walser M. Phenomenological analysis of electrolyte homeostasis. In: Seldin DW, Giebisch G, eds. *The Kidney: Physiology and Pathophysiology (Vols 1–3)*. New York, New York: Raven Press, Ltd; 1992:31–44.
4. Rakova N, et al. Increased salt consumption induces body water conservation and decreases fluid intake. *J Clin Invest*. 2017;127(5):1932–1943.
5. Sanchez AM, Candau RB, Csibi A, Pagano AF, Raibon A, Bernardi H. The role of AMP-activated protein kinase in the coordination of skeletal muscle turnover and energy homeostasis. *Am J Physiol, Cell Physiol*. 2012;303(5):C475–C485.
6. Cheung PC, Salt IP, Davies SP, Hardie DG, Carling D. Characterization of AMP-activated protein kinase gamma-subunit isoforms and their role in AMP binding. *Biochem J*. 2000;346 Pt 3:659–669.
7. Hardie DG. Sensing of energy and nutrients by AMP-activated protein kinase. *Am J Clin Nutr*. 2011;93(4):891S–8916.
8. Carling D, Clarke PR, Zammit VA, Hardie DG. Purification and characterization of the AMP-activated protein kinase. Copurification of acetyl-CoA carboxylase kinase and 3-hydroxy-3-methylglutaryl-CoA reductase kinase activities. *Eur J Biochem*. 1989;186(1–2):129–136.
9. Mammucari C, et al. FoxO3 controls autophagy in skeletal muscle in vivo. *Cell Metab*. 2007;6(6):458–471.
10. Sanchez AM, et al. AMPK promotes skeletal muscle autophagy through activation of forkhead FoxO3a and interaction with Ulk1. *J Cell Biochem*. 2012;113(2):695–710.
11. Merrill GF, Kurth EJ, Hardie DG, Winder WW. AICA riboside increases AMP-activated protein kinase, fatty acid oxidation, and glucose uptake in rat muscle. *Am J Physiol*. 1997; 273(6 Pt 1):E1107–E1112.
12. Winder WW, Hardie DG. Inactivation of acetyl-CoA carboxylase and activation of AMP-activated protein kinase in muscle during exercise. *Am J Physiol*. 1996;270(2 Pt 1):E299–E304.
13. Winder WW, et al. Phosphorylation of rat muscle acetyl-CoA carboxylase by AMP-activated protein kinase and protein kinase A. *J Appl Physiol*. 1997;82(1):219–225.
14. McGarry JD, Brown NF. The mitochondrial carnitine palmitoyltransferase system. From concept to molecular analysis. *Eur J Biochem*. 1997;244(1):1–14.
15. Storey KB, Storey JM. Aestivation: signaling and hypometabolism. *J Exp Biol*. 2012; 215(Pt 9):1425–1433.
16. Delaney RG, Lahiri S, Fishman AP. Aestivation of the African lungfish Protopterus aethiopicus: cardiovascular and respiratory functions. *J Exp Biol*. 1974;61(1):111–128.
17. Walser M. Phenomenological analysis of renal regulation of sodium and potassium balance. *Kidney Int*. 1985;27(6):837–841.
18. Gamble JL, McKhann CF, Butler AM, Tuthill E. An economy of water in renal function referable to urea. *Am J Physiol*. 1934;109(1):139–154.
19. Fenton RA, Chou CL, Sowersby H, Smith CP, Knepper MA. Gamble's "economy of water" revisited: studies in urea transporter knockout mice. *Am J Physiol Renal Physiol*. 2006;291(1):F148–F154.
20. Weiner ID, Mitch WE, Sands JM. Urea and ammonia metabolism and the control of renal nitrogen excretion. *Clin J Am Soc Nephrol*. 2015;10(8):1444–1458.
21. Kim YM, et al. Urea and NaCl regulate UT-A1 urea transporter in opposing directions via TonEBP pathway during osmotic diuresis. *Am J Physiol Renal Physiol*. 2009;296(1):F67–F77.
22. Perucca J, Bouby N, Valeix P, Bankir L. Sex difference in urine concentration across differing ages, sodium intake, and level of kidney disease. *Am J Physiol Regul Integr Comp Physiol*. 2007;292(2):R700–R705.
23. de Blaauw I, Deutz NE, Von Meyenfeldt MF. In vivo amino acid metabolism of gut and liver during short and prolonged starvation. *Am J Physiol*. 1996;270(2 Pt 1):G298–G306.
24. Felig P, Owen OE, Wahren J, Cahill GF. Amino acid metabolism during prolonged starvation. *J Clin Invest*. 1969;48(3):584–594.
25. Felig P. The glucose-alanine cycle. *Metab Clin Exp*. 1973;22(2):179–207.
26. Smith HW. Metabolism of the lung-fish, protopterus aethiopicus. *J Biol Chem*. 1930;88(1):97–120.
27. Loong AM, Hiong KC, Lee SM, Wong WP, Chew SF, Ip YK. Ornithine-urea cycle and urea synthesis in African lungfishes, Protopterus aethiopicus and Protopterus annectens, exposed to terrestrial

conditions for six days. *J Exp Zoolog Part A Comp Exp Biol*. 2005;303(5):354–365.
28. Wilkie MP, et al. The African lungfish (Protopterus dolloi): ionoregulation and osmoregulation in a fish out of water. *Physiol Biochem Zool*. 2007;80(1):99–112.
29. Loong AM, Hiong KC, Wong WP, Chew SF, Ip YK. Differential gene expression in the liver of the African lungfish, Protopterus annectens, after 6 days of estivation in air. *J Comp Physiol B, Biochem Syst Environ Physiol*. 2012;182(2):231–245.
30. Hiong KC, Ip YK, Wong WP, Chew SF. Differential gene expression in the liver of the African lungfish, Protopterus annectens, after 6 months of aestivation in air or 1 day of arousal from 6 months of aestivation. *PLoS One*. 2015;10(3):e0121224.
31. Ramnanan CJ, McMullen DC, Groom AG, Storey KB. The regulation of AMPK signaling in a natural state of profound metabolic rate depression. *Mol Cell Biochem*. 2010;335(1–2):91–105.
32. Szidon JP, Lahiri S, Lev M, Fishman AP. Heart and circulation of the African lungfish. *Circ Res*. 1969;25(1):23–38.
33. Stenvinkel P, et al. Metabolic changes in summer active and anuric hibernating free-ranging brown bears (Ursus arctos). *PLoS One*. 2013;8(9):e72934.
34. Naruse M, Klein JD, Ashkar ZM, Jacobs JD, Sands JM. Glucocorticoids downregulate the vasopressin-regulated urea transporter in rat terminal inner medullary collecting ducts. *J Am Soc Nephrol*. 1997;8(4):517–523.
35. Evans AM, DeHaven CD, Barrett T, Mitchell M, Milgram E. Integrated, nontargeted ultrahigh performance liquid chromatography/electrospray ionization tandem mass spectrometry platform for the identification and relative quantification of the small-molecule complement of biological systems. *Anal Chem*. 2009;81(16):6656–6667.
36. Mizushima N, Yamamoto A, Matsui M, Yoshimori T, Ohsumi Y. In vivo analysis of autophagy in response to nutrient starvation using transgenic mice expressing a fluorescent autophagosome marker. *Mol Biol Cell*. 2004;15(3):1101–1111.
37. Wiig H, et al. Immune cells control skin lymphatic electrolyte homeostasis and blood pressure. *J Clin Invest*. 2013;123(7):2803–2815.